THE JOURNAL OF PHYSICAL CHEMISTRY Letters

Letter

pubs.acs.org/JPCL

Label-Free Vibrational Spectroscopic Imaging of Neuronal Membrane Potential

Hyeon Jeong Lee,[†,‡,⊥] Delong Zhang,[†,⊥] Ying Jiang,[†,‡] Xiangbing Wu,[§] Pei-Yu Shih,[#] Chien-Sheng Liao,[†] Brittani Bungart,[†,∥] Xiao-Ming Xu,[§] Ryan Drenan,[#,▽] Edward Bartlett,[†,‡] and Ji-Xin Cheng*[,†,‡,¶]

[†]Weldon School of Biomedical Engineering, Purdue University, West Lafayette, Indiana 47907-2032, United States

[‡]Interdisciplinary Life Science Program, Purdue University, West Lafayette, Indiana 47907, United States

[§]Stark Neurosciences Research Institute, Indiana University School of Medicine, Indianapolis, Indiana 46202-2266, United States

[#]Medicinal Chemistry and Molecular Pharmacology, Purdue University, West Lafayette, Indiana 47907, United States

[∥]MD PhD Program, Indiana University School of Medicine, Indianapolis, Indiana 46202-5120, United States

[¶]Department of Chemistry, Purdue University, West Lafayette, Indiana 47907-2084, United States

Supporting Information

ABSTRACT: Detecting membrane potentials is critical for understanding how neuronal networks process information. We report a vibrational spectroscopic signature of neuronal membrane potentials identified through hyperspectral stimulated Raman scattering (SRS) imaging of patched primary neurons. High-speed SRS imaging allowed direct visualization of puff-induced depolarization of multiple neurons in mouse brain slices, confirmed by simultaneous calcium imaging. The observed signature, partially dependent on sodium ion influx, is interpreted as ion interactions on the CH_3 Fermi resonance peak in proteins. By implementing a dual-SRS balanced detection scheme, we detected single action potentials in electrically stimulated neurons. These results collectively demonstrate the potential of sensing neuronal activities at multiple sites with a label-free vibrational microscope.

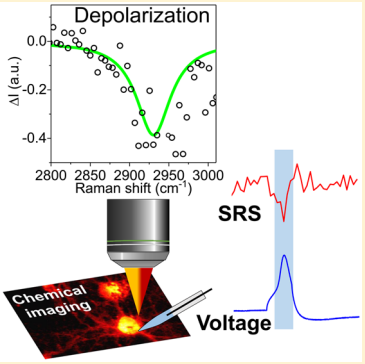

Membrane potential is a critical regulator of neuronal excitability, calcium influx, and plasticity. Its differential distributions in soma, dendrites, and axon lead to spatially segregated processing.[1] Thus, imaging membrane potential with submicrometer spatial resolution and millisecond temporal resolution has been pursued as a long-term goal of neuroscience.[2] Optical recording methods offer potentially less invasive, better targeted, and far greater multisite monitoring capability than conventional patch clamp measurements.[3,4] Today, the most widely adopted methods are based on fluorescent voltage indicators, including voltage-sensitive dyes[4−6] and voltage-sensitive fluorescent proteins.[7−10] To date, voltage sensors have reached 2 ms response time to resolve fast spiking[11] and demonstrated neuron imaging at the single-cell level in small model organisms.[12,13]

In parallel to fluorescence approaches, label-free methods are continuously sought for detecting membrane potentials with the advantage of simple sample preparation, low toxicity, and no photobleaching.[14] In 1949, Hill and Keynes[15] observed changes in light scattering from an activated nerve. Cohen et al. recorded action potentials on a squid giant axon using changes in light scattering and birefringence.[16] Stepnoski et al. detected membrane potentials in an individual invertebrate cell using angle-resolved light scattering.[17] For mammalian neurons, which are smaller and more transparent, light scattering-based membrane potential measurement was demonstrated only in a group of cells or nerve terminals.[18−24] Spatial distribution of membrane potential-related optical properties of single non-neuronal cells was demonstrated by optical interferometric microscopy.[25] However, these linear optical processes suffer from limited longitudinal sectioning capability. Nonlinear, self-phase modulation was recently reported as an intrinsic contrast to sense electrical activity in hippocampal brain slices.[26] To date, label-free imaging of action potentials in a single neuron has not been achieved.

Vibrational spectroscopy based on quantized motions of chemical bonds and/or functional groups provides sensitive measurements of microenvironment, including pH, electric field, and solvent shell of ions.[27−29] By offering a large signal level, stimulated Raman scattering (SRS) microscopy[30−33] has enabled high-speed vibrational imaging for cell metabolism studies and in vivo cancer detection.[34,35] By providing a spectrum at each pixel, recently developed hyperspectral SRS microscopy has enabled chemical imaging of cells, tissues, and model organisms based on the spectral signatures of biomolecules.[36−41] Toward functional measurement, SRS imaging of a static erythrocyte ghost model showed a

Received: March 8, 2017
Accepted: April 13, 2017
Published: April 13, 2017

DOI: 10.1021/acs.jpclett.7b00575
J. Phys. Chem. Lett. 2017, 8, 1932−1936

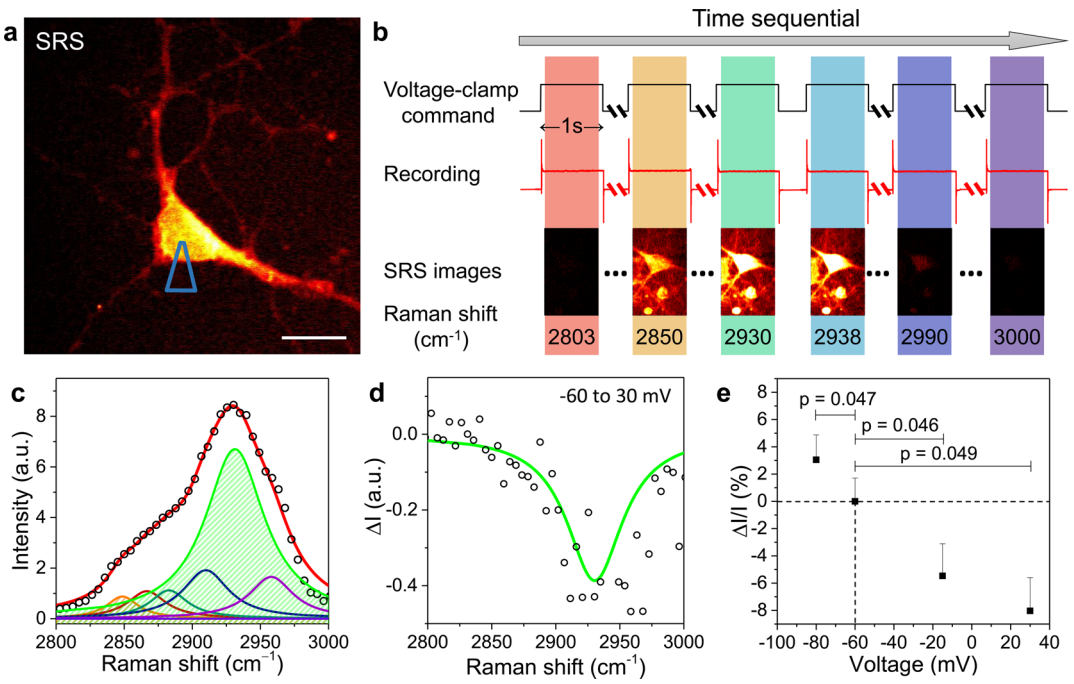

Figure 1. (a) SRS image of a patched neuron with micropipette position indicated. Scale bar: 10 μm. (b) Schematic of hyperspectral SRS imaging of neurons while holding different potentials. (c) Representative SRS spectrum of a patched neuron (dot), fitted using seven Lorentzian (colored lines) with major contributing bands filled, 2850 (orange) and 2930 cm^{-1} (green). Red: cumulative fitted curve. (d) SRS spectral change, ΔI (dots), of the neuron from −60 to +30 mV with fitted curve (line). (e) Percentage changes of SRS intensity ($\Delta I/I$) of neurons at 2930 cm^{-1} at various membrane potentials. Error bars: + standard error of the mean (SEM).

correlation of membrane spectral profile with transmembrane potential.[42] In this work, we report an intrinsic spectroscopic signature of membrane potential identified through hyperspectral SRS imaging of live neurons.

To search for the spectroscopic signature of membrane potential, we deployed frame-by-frame hyperspectral SRS imaging with a spectral focusing approach[43] and mapped primary neurons under somatic voltage-clamp control (Figure 1a,b and Figure S1). Four different membrane potentials were applied: near typical resting potential at −60 mV, two depolarized potentials at −15 and +30 mV, and hyperpolarization potential at −80 mV. Because C−H bonds are the most abundant functional groups in cells, our study focused at the high wavenumber C−H stretching region (2800−3000 cm^{-1}). The two distinctive Raman bands are the symmetric CH_2 vibration at 2850 cm^{-1}, mainly contributed by acyl chains in lipids, and the CH_3 vibration at 2930 cm^{-1}, mainly contributed by amino acid side chains in proteins (Figure 1c). By analysis of the hyperspectral image stacks on the same neuron, we found a significant decrease in SRS intensity at 2930 cm^{-1} in depolarized neuron (Figure 1d), while SRS intensity at 2850 cm^{-1} remains unchanged (Figure S2). Furthermore, SRS intensity at 2930 cm^{-1} increased in hyperpolarized neuron (Figure S3). The change of SRS intensity at 2930 cm^{-1} was repeatable in multiple neurons (Figure 1e). These results demonstrate the SRS peak at 2930 cm^{-1} as a vibrational signature of neuronal membrane potential.

To demonstrate the capability of multisite measurement, SRS imaging of a whole neuron was performed during voltage clamping (Figure S4a). The SRS intensity change at 2930 cm^{-1} in depolarized neuron was obtained from the spectroscopic imaging stacks (Figure S4b,c). The SRS intensity showed a clear drop in the regions near the micropipette but smaller or no change in the regions further away from the micropipette (Figure S4d). This result provides visual evidence of the lack of space-clamp, a phenomenon in which voltage clamp becomes less reliable in regions further from the micropipette tip.[44]

We further demonstrated real-time SRS imaging of neuronal depolarization in brain slices induced by KCl, delivered through a nearby puffing pipet. Simultaneous two-photon fluorescence imaging of Fura-2 AM calcium indicator was used to evaluate the neuronal response (Figure 2a). The KCl puffing resulted in

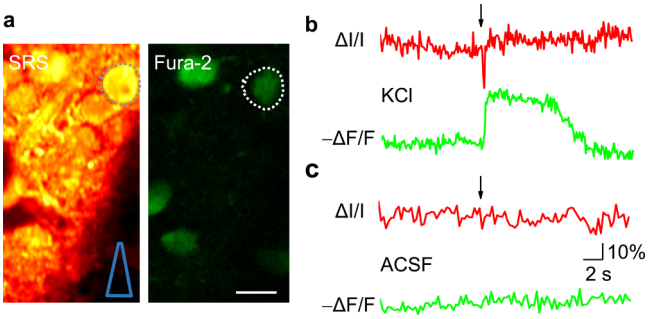

Figure 2. (a) Representative SRS and Fura-2 fluorescence images of the medial habenula region in a live mouse brain slice. (b) Time traces of SRS and fluorescence signals of the neuron indicated in panel a, when puffing KCl. (c) The same neuron when puffing ACSF. The time point of puffing is indicated by an arrow.

calcium influx in the neuron, indicated by a decrease in fluorescence intensity (Figure 2b). A sharp dip in SRS intensity, indicative of membrane depolarization, was observed immediately prior to the calcium response upon the KCl stimulation (Figure 2b), indicating the superior temporal resolution offered by membrane potential recording. We note that current voltage-sensitive probes reach a response time of several

DOI: 10.1021/acs.jpclett.7b00575
J. Phys. Chem. Lett. 2017, 8, 1932−1936

milliseconds.[11,45] Nevertheless, because the calcium ions accumulate much slower, an elongated response curve is observed. Neither Fura-2 nor SRS intensity changes were observed in the control, in which the same neurons were puffed with an artificial cerebrospinal fluid buffer (Figure 2c). Furthermore, we examined multiple cells in hippocampus regions (Figure S5), in which only neurons displaying a calcium response showed changes in SRS intensity (Figure S5c–e).

To elucidate the spatial origin of the vibrational signature, we compared the SRS time-trace in the near-membrane region to that in the intracellular area. The near-membrane region was shown to contribute most of the SRS dip upon depolarization, while the intracellular region did not show an obvious decrease in the SRS intensity at 2930 cm^{-1} (Figure S6). Similarly, we found a smaller decrease of SRS intensity in the intracellular area in Figure S4 (regions 19 and 27) compared to the cell edges (regions 13 to 18). These observations indicate that the near-membrane molecules mainly contribute the observed signature.

Voltage-gated sodium channels are one of the major proteins responsible for initiation of action potentials. To determine whether voltage-gated sodium channels play a role in the SRS spectral profile change, we used tetrodotoxin (TTX) to block these channels. Addition of TTX blocked the fast inward sodium current as indicated from the electrical recording (Figure S7). Before TTX treatment, the SRS intensity at 2930 cm^{-1} decreased when a depolarized potential was applied to the neuron (Figure 3a). The repeated measurement of the SRS spectral profile at the resting potential had no significant change compared to the initial profile, indicating stability of the whole-cell patch and minimal photodamage. We found a reduced change in SRS intensity with TTX applied to the extracellular buffer (Figure 3b), suggesting that voltage-gated sodium channels partially contribute to Raman spectral profile change.

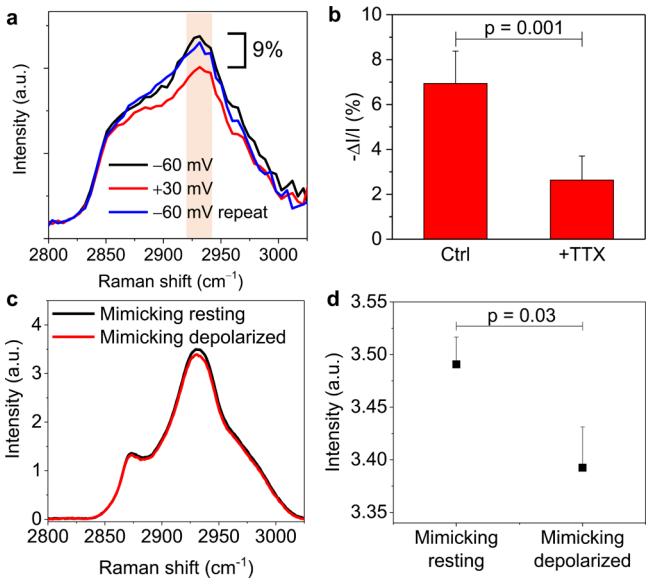

Figure 3. (a) SRS spectra of a neuron recorded at −60 and +30 mV. (b) Percentage changes of SRS intensity ($\Delta I/I$) of neurons at 2930 cm^{-1} at +30 mV before and after being treated with 3 μM TTX. (c) Raman spectra of bovine serum albumin (190 mg/mL) dissolved in different ionic compositions. Resting potential-mimicking buffer, 18 mM NaCl + 135 mM KCl; depolarized potential-mimicking buffer, 150 mM NaCl + 135 mM KCl (see the Supporting Information). (d) Raman intensities at 2930 cm^{-1} of BSA in panel c. Error bars: +SEM.

It is difficult but important to understand the mechanism of the vibrational spectroscopic signature of membrane voltage in the complex neuronal environment at a millisecond scale. Our hypothesis focuses on the CH_3 Fermi resonance peak of proteins, the major content in near-membrane cytosol. Specifically, the 2930 cm^{-1} peak is the Fermi resonance between the overtone of the CH_3 bending mode and the CH_3 stretching mode in the 2850–3000 cm^{-1} region.[46,47] The Fermi resonance peak is sensitive to molecular environment and has been employed as a probe of chemical environment.[48] Recent in silico studies of Fermi resonance in C–H stretching vibration modes also demonstrated the effect.[49] Upon neuron firing, the rapid ion exchange, primarily sodium ion influx, drastically changes the local environment of near-membrane proteins, which interferes with the Fermi coupling of the 2930 cm^{-1} peak and reduces the peak intensity. To test the hypothesis, we recorded Raman spectra of protein in solutions mimicking the physiological near-membrane conditions during depolarization and compared them to those at resting state (Figure 3c,d). The intensity of the 2930 cm^{-1} peak decreased significantly at the depolarizing condition. Additionally, we observed an increase in the spectral separation between the two peaks (Figure S8), indicating the weakening of Fermi coupling. These findings are consistent with our hypothesis. We also note that the SRS intensity drop was reduced by 57% when sodium channels were blocked in neurons (Figure 3b), indicating the importance of sodium influx in the process. Meanwhile, the remaining changes of the spectroscopic signature were possibly attributable to other ions.

It is worth noting that molecular reorientation is a possible cause for the spectral changes. However, in our experiments, we did not find anisotropic spectral features to support this possibility. Notably, at diffraction-limited spatial resolution, our SRS imaging technology probes not only the plasma membrane but also biomolecules inside and outside the cell. Nevertheless, it is unlikely that the observed SRS intensity change arises from proteins in the extracellular matrix because the effect of an action potential on the extracellular Na^+ concentration is negligible because of the large sodium pool. Also, the observed instantaneous change of SRS intensity upon chemical or electrical stimulation is unlikely a consequence of metabolic response inside cells. Another possibility accounting for the SRS intensity drop is the spatial shift of neuron bodies. Previous studies show that neurons swell on the scale of 0.1 nm when firing action potentials,[50] which is negligible in optical microscopy. Additionally, physical swelling or shrinking of a cell will not cause spectral changes. However, we note that a change in protein density due to local swelling or shrinking might contribute to the spectral change. Altogether, SRS imaging at the Fermi resonance peak offers a unique approach to monitor the membrane voltage in real time with submicrometer spatial resolution.

To resolve single action potentials, we performed line-scan imaging of a patched neuron at a speed of 1000 line/s with newly designed dual-SRS balanced detection (Figure S9a and Methods in the Supporting Information). In short, we split a small portion of the excitation lasers to generate an additional SRS signal of a standard sample to monitor the stochastic noise of the system. By this approach, the stochastic noise spikes in a resting neuron were completely removed, improving the overall standard deviation of the SRS trace from 2% to less than 0.5%

DOI: 10.1021/acs.jpclett.7b00575
J. Phys. Chem. Lett. 2017, 8, 1932–1936

of the average SRS intensity (Figure S9b). An intensity drop in accordance with the intracellularly recorded membrane voltage was found (Figure 4). The measured signal-to-noise ratio of the

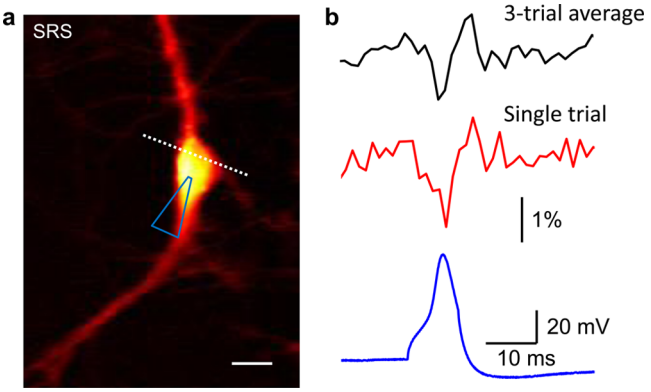

Figure 4. (a) SRS image of a patched neuron. The dashed line indicates the scanning trace. (b) 3-trial average (black) and single-trial SRS time trace (red) of the neuron shown in panel a with simultaneous current clamp recording (blue), showing a single action potential. The SRS intensity was normalized by the SRS reference generated with the same pulses. Scale bar: 20 μm.

dual-SRS trace was 3.6 without averaging. Importantly, we observed an overshoot after the dip, which coincided with the hyperpolarization shown in the electrical recording (Figure 4b). These time-resolved features are consistent with the spectroscopic signature of membrane potential shown in Figure 1e.

In conclusion, by SRS imaging at a Fermi resonance peak, we demonstrated label-free mapping of membrane potential throughout a recorded neuron. Our method can be potentially used for evaluating neuronal excitability, investigating dendritic integration and neural plasticity, or identifying neuronal compartments most affected in ion channel disorders. With improvement in imaging speed, our method will further enable label-free evaluation of membrane potential with multineuron, multisite, and long-term measurement capabilities.

■ ASSOCIATED CONTENT

Supporting Information

The Supporting Information is available free of charge on the ACS Publications website at DOI: 10.1021/acs.jpclett.7b00575.

Methods for primary neuronal cell culture, electrophysiology, SRS imaging, dual-SRS balanced detection, line-scan SRS imaging, brain slice preparation, synchronous SRS and two-photon fluorescence imaging, Raman spectral analysis of bovine serum albumin in ionic solutions, and statistical analysis; Figures S1−S9 (PDF)

■ AUTHOR INFORMATION

Corresponding Author

*E-mail: jcheng@purdue.edu.

ORCID

Delong Zhang: 0000-0002-9734-3573

Ji-Xin Cheng: 0000-0002-5607-6683

Present Address

[▽]R.D.: Department of Pharmacology, Northwestern University Feinberg School of Medicine, Chicago, IL.

Author Contributions

[⊥]H.J.L. and D.Z. contributed equally.

Notes

The authors declare no competing financial interest.

■ ACKNOWLEDGMENTS

The authors thank Bin Liu and Adam Anderson for help in the experiments and Staci Engle for demonstration of the patch clamp procedure. J.-X.C. thanks Na Ji for stimulation of label-free spectroscopic imaging of membrane voltage. This work was supported by a Keck Foundation Science and Engineering grant to J.-X.C., a Brain and Behavior Research Foundation Young Investigator Award to R.D., and R00DA030396 to R.D. B.B. acknowledges the Medical Scientist Training Program Grant T32 GM077229 from NIH.

■ REFERENCES

(1) Nusser, Z. Variability in the subcellular distribution of ion channels increases neuronal diversity. *Trends Neurosci.* **2009**, *32*, 267.
(2) Yuste, R. From the neuron doctrine to neural networks. *Nat. Rev. Neurosci.* **2015**, *16*, 487.
(3) Scanziani, M.; Hausser, M. Electrophysiology in the age of light. *Nature* **2009**, *461*, 930.
(4) Peterka, D. S.; Takahashi, H.; Yuste, R. Imaging voltage in neurons. *Neuron* **2011**, *69*, 9.
(5) Grinvald, A.; Hildesheim, R. VSDI: a new era in functional imaging of cortical dynamics. *Nat. Rev. Neurosci.* **2004**, *5*, 874.
(6) Miller, E. W.; Lin, J. Y.; Frady, E. P.; Steinbach, P. A.; Kristan, W. B., Jr.; Tsien, R. Y. Optically monitoring voltage in neurons by photo-induced electron transfer through molecular wires. *Proc. Natl. Acad. Sci. U. S. A.* **2012**, *109*, 2114.
(7) Akemann, W.; Mutoh, H.; Perron, A.; Rossier, J.; Knopfel, T. Imaging brain electric signals with genetically targeted voltage-sensitive fluorescent proteins. *Nat. Methods* **2010**, *7*, 643.
(8) Jin, L.; Han, Z.; Platisa, J.; Wooltorton, J. R.; Cohen, L. B.; Pieribone, V. A. Single action potentials and subthreshold electrical events imaged in neurons with a fluorescent protein voltage probe. *Neuron* **2012**, *75*, 779.
(9) Hochbaum, D. R.; Zhao, Y.; Farhi, S. L.; Klapoetke, N.; Werley, C. A.; Kapoor, V.; Zou, P.; Kralj, J. M.; Maclaurin, D.; Smedemark-Margulies, N.; Saulnier, J. L.; Boulting, G. L.; Straub, C.; Cho, Y. K.; Melkonian, M.; Wong, G. K.; Harrison, D. J.; Murthy, V. N.; Sabatini, B. L.; Boyden, E. S.; Campbell, R. E.; Cohen, A. E. All-optical electrophysiology in mammalian neurons using engineered microbial rhodopsins. *Nat. Methods* **2014**, *11*, 825.
(10) St-Pierre, F.; Chavarha, M.; Lin, M. Z. Designs and sensing mechanisms of genetically encoded fluorescent voltage indicators. *Curr. Opin. Chem. Biol.* **2015**, *27*, 31.
(11) St-Pierre, F.; Marshall, J. D.; Yang, Y.; Gong, Y.; Schnitzer, M. J.; Lin, M. Z. High-fidelity optical reporting of neuronal electrical activity with an ultrafast fluorescent voltage sensor. *Nat. Neurosci.* **2014**, *17*, 884.
(12) Cao, G.; Platisa, J.; Pieribone, V. A.; Raccuglia, D.; Kunst, M.; Nitabach, M. N. Genetically Targeted Optical Electrophysiology in Intact Neural Circuits. *Cell* **2013**, *154*, 904.
(13) Flytzanis, N. C.; Bedbrook, C. N.; Chiu, H.; Engqvist, M. K.; Xiao, C.; Chan, K. Y.; Sternberg, P. W.; Arnold, F. H.; Gradinaru, V. Archaerhodopsin variants with enhanced voltage-sensitive fluorescence in mammalian and Caenorhabditis elegans neurons. *Nat. Commun.* **2014**, *5*, 4894.
(14) Baker, M. Laser tricks without labels. *Nat. Methods* **2010**, *7*, 261.
(15) Hill, D. K.; Keynes, R. D. Opacity changes in stimulated nerve. *J. Physiol.* **1949**, *108*, 278.
(16) Cohen, L. B.; Keynes, R. D.; Hille, B. Light scattering and birefringence changes during nerve activity. *Nature* **1968**, *218*, 438.
(17) Stepnoski, R. A.; LaPorta, A.; Raccuia-Behling, F.; Blonder, G. E.; Slusher, R. E.; Kleinfeld, D. Noninvasive detection of changes in membrane potential in cultured neurons by light scattering. *Proc. Natl. Acad. Sci. U. S. A.* **1991**, *88*, 9382.

DOI: 10.1021/acs.jpclett.7b00575
J. Phys. Chem. Lett. 2017, 8, 1932−1936

(18) Salzberg, B. M.; Obaid, A. L.; Gainer, H. Large and rapid changes in light scattering accompany secretion by nerve terminals in the mammalian neurohypophysis. *J. Gen. Physiol.* **1985**, *86*, 395.
(19) Salzberg, B. M.; Obaid, A. L. Optical studies of the secretory event at vertebrate nerve terminals. *J. Exp. Biol.* **1988**, *139*, 195.
(20) Rector, D. M.; Poe, G. R.; Kristensen, M. P.; Harper, R. M. Light scattering changes follow evoked potentials from hippocampal Schaeffer collateral stimulation. *J. Neurophysiol.* **1997**, *78*, 1707.
(21) Rector, D. M.; Rogers, R. F.; Schwaber, J. S.; Harper, R. M.; George, J. S. Scattered-light imaging in vivo tracks fast and slow processes of neurophysiological activation. *NeuroImage* **2001**, *14*, 977.
(22) Rector, D. M.; Carter, K. M.; Volegov, P. L.; George, J. S. Spatio-temporal mapping of rat whisker barrels with fast scattered light signals. *NeuroImage* **2005**, *26*, 619.
(23) Tsytsarev, V.; Premachandra, K.; Takeshita, D.; Bahar, S. Imaging cortical electrical stimulation in vivo: fast intrinsic optical signal versus voltage-sensitive dyes. *Opt. Lett.* **2008**, *33*, 1032.
(24) Badreddine, A. H.; Jordan, T.; Bigio, I. J. Real-time imaging of action potentials in nerves using changes in birefringence. *Biomed. Opt. Express* **2016**, *7*, 1966.
(25) Oh, S.; Fang-Yen, C.; Choi, W.; Yaqoob, Z.; Fu, D.; Park, Y.; Dassari, R. R.; Feld, M. S. Label-free imaging of membrane potential using membrane electromotility. *Biophys. J.* **2012**, *103*, 11.
(26) Fischer, M. C.; Liu, H. C.; Piletic, I. R.; Escobedo-Lozoya, Y.; Yasuda, R.; Warren, W. S. Self-phase modulation signatures of neuronal activity. *Opt. Lett.* **2008**, *33*, 219.
(27) Verma, S. P.; Wallach, D. F. Erythrocyte membranes undergo cooperative, pH-sensitive state transitions in the physiological temperature range: evidence from Raman spectroscopy. *Proc. Natl. Acad. Sci. U. S. A.* **1976**, *73*, 3558.
(28) Mikkelsen, R. B.; Verma, S. P.; Wallach, D. F. Effect of transmembrane ion gradients on Raman spectra of sealed, hemoglobin-free erythrocyte membrane vesicles. *Proc. Natl. Acad. Sci. U. S. A.* **1978**, *75*, 5478.
(29) Davis, J. G.; Gierszal, K. P.; Wang, P.; Ben-Amotz, D. Water structural transformation at molecular hydrophobic interfaces. *Nature* **2012**, *491*, 582.
(30) Ploetz, E.; Laimgruber, S.; Berner, S.; Zinth, W.; Gilch, P. Femtosecond stimulated Raman microscopy. *Appl. Phys. B: Lasers Opt.* **2007**, *87*, 389.
(31) Freudiger, C. W.; Min, W.; Saar, B. G.; Lu, S.; Holtom, G. R.; He, C.; Tsai, J. C.; Kang, J. X.; Xie, X. S. Label-free biomedical imaging with high sensitivity by stimulated Raman scattering microscopy. *Science* **2008**, *322*, 1857.
(32) Nandakumar, P.; Kovalev, A.; Volkmer, A. Vibrational imaging based on stimulated Raman scattering microscopy. *New J. Phys.* **2009**, *11*, 033026.
(33) Ozeki, Y.; Dake, F.; Kajiyama, S.; Fukui, K.; Itoh, K. Analysis and experimental assessment of the sensitivity of stimulated Raman scattering microscopy. *Opt. Express* **2009**, *17*, 3651.
(34) Cheng, J. X.; Xie, X. S. Vibrational spectroscopic imaging of living systems: An emerging platform for biology and medicine. *Science* **2015**, *350*, aaa8870.
(35) Ji, M.; Orringer, D. A.; Freudiger, C. W.; Ramkissoon, S.; Liu, X.; Lau, D.; Golby, A. J.; Norton, I.; Hayashi, M.; Agar, N. Y.; Young, G. S.; Spino, C.; Santagata, S.; Camelo-Piragua, S.; Ligon, K. L.; Sagher, O.; Xie, X. S. Rapid, label-free detection of brain tumors with stimulated Raman scattering microscopy. *Sci. Transl. Med.* **2013**, *5*, 201.
(36) Ozeki, Y.; Umemura, W.; Otsuka, Y.; Satoh, S.; Hashimoto, H.; Sumimura, K.; Nishizawa, N.; Fukui, K.; Itoh, K. High-speed molecular spectral imaging of tissue with stimulated Raman scattering. *Nat. Photonics* **2012**, *6*, 845.
(37) Zhang, D.; Wang, P.; Slipchenko, M. N.; Ben-Amotz, D.; Weiner, A. M.; Cheng, J. X. Quantitative vibrational imaging by hyperspectral stimulated Raman scattering microscopy and multivariate curve resolution analysis. *Anal. Chem.* **2013**, *85*, 98.
(38) Fu, D.; Holtom, G.; Freudiger, C.; Zhang, X.; Xie, X. S. Hyperspectral imaging with stimulated Raman scattering by chirped femtosecond lasers. *J. Phys. Chem. B* **2013**, *117*, 4634.
(39) Wang, P.; Li, J.; Hu, C. R.; Zhang, D.; Sturek, M.; Cheng, J. X. Label-free quantitative imaging of cholesterol in intact tissues by hyperspectral stimulated Raman scattering microscopy. *Angew. Chem., Int. Ed.* **2013**, *52*, 13042.
(40) Wang, P.; Liu, B.; Zhang, D.; Belew, M. Y.; Tissenbaum, H. A.; Cheng, J. X. Imaging lipid metabolism in live Caenorhabditis elegans using fingerprint vibrations. *Angew. Chem., Int. Ed.* **2014**, *53*, 11787.
(41) Liao, C.-S.; Huang, K.-C.; Hong, W.; Chen, A. J.; Karanja, C.; Wang, P.; Eakins, G.; Cheng, J.-X. Stimulated Raman spectroscopic imaging by microsecond delay-line tuning. *Optica* **2016**, *3*, 1377.
(42) Liu, B.; Lee, H. J.; Zhang, D.; Liao, C.-S.; Ji, N.; Xia, Y.; Cheng, J.-X. Label-free spectroscopic detection of membrane potential using stimulated Raman scattering. *Appl. Phys. Lett.* **2015**, *106*, 173704.
(43) Andresen, E. R.; Berto, P.; Rigneault, H. Stimulated Raman scattering microscopy by spectral focusing and fiber-generated soliton as Stokes pulse. *Opt. Lett.* **2011**, *36*, 2387.
(44) Bar-Yehuda, D.; Korngreen, A. Space-clamp problems when voltage clamping neurons expressing voltage-gated conductances. *J. Neurophysiol.* **2008**, *99*, 1127.
(45) Vogt, N. Voltage sensors: challenging, but with potential. *Nat. Methods* **2015**, *12*, 921.
(46) Gan, W.; Zhang, Z.; Feng, R.-r.; Wang, H.-f. Identification of overlapping features in the sum frequency generation vibrational spectra of air/ethanol interface. *Chem. Phys. Lett.* **2006**, *423*, 261.
(47) Yu, Y.; Lin, K.; Zhou, X.; Wang, H.; Liu, S.; Ma, X. New C−H stretching vibrational spectral features in the Raman spectra of gaseous and liquid ethanol. *J. Phys. Chem. C* **2007**, *111*, 8971.
(48) Kish, E.; Pinto, M. M. M.; Bovi, D.; Basire, M.; Guidoni, L.; Vuilleumier, R.; Robert, B.; Spezia, R.; Mezzetti, A. Fermi Resonance as a Tool for Probing Peridinin Environment. *J. Phys. Chem. B* **2014**, *118*, 5873.
(49) Sibert, E. L.; Tabor, D. P.; Lisy, J. M. Modeling the CH Stretch Vibrational Spectroscopy of M+[Cyclohexane] (M = Li, Na, and K) Ions. *J. Phys. Chem. A* **2015**, *119*, 10293.
(50) Iwasa, K.; Tasaki, I.; Gibbons, R. C. Swelling of nerve fibers associated with action potentials. *Science* **1980**, *210*, 338.

DOI: 10.1021/acs.jpclett.7b00575
J. Phys. Chem. Lett. 2017, 8, 1932−1936